Available online at www.sciencedirect.com
SCIENCE DIRECT
ELSEVIER
Polymer 47 (2006) 2263–2268
polymer
www.elsevier.com/locate/polymer

Polymer Communication

In situ monitoring of mechanical properties during photopolymerization with particle tracking microrheology

Ryan P. Slopek, Haris K. McKinley, Clifford L. Henderson, Victor Breedveld *

School of Chemical & Biomolecular Engineering, Georgia Institute of Technology, Atlanta, GA 30332-0100, USA

Received 14 October 2005; received in revised form 27 January 2006; accepted 30 January 2006
Available online 28 February 2006

Abstract

Microrheology was employed to perform in situ monitoring of the liquid-to-gel transition during free-radical photopolymerization. Photosensitive acrylate resins were exposed to ultraviolet light, while the Brownian motion of micrometer sized, inert fluorescent tracer particles was tracked via optical videomicroscopy. Statistical analysis of particle motion yielded the rheological properties of the embedding medium as a function of time and location, thereby relating UV exposure to the progress of polymerization and gelation. Microscopy enabled a detailed study of three-dimensional gelation profiles; other experimental parameters that were varied include photoinitiator concentration, monomer composition, the presence of oxygen and light intensity. Significant changes in gelation time were observed with increasing distance from the illuminated surface into the sample under all conditions. The results were used to test the accuracy of the standard energy threshold model, which is often used to empirically predict the outcome of photopolymerization reactions.

Keywords: Microrheology; Photopolymerization; Kinetic modeling

1. Introduction

The UV activated polymerization of multifunctional liquid monomers enhanced with photoinitiator is one of the most effective techniques used to create solid polymeric coatings and objects. The resulting highly cross-linked solid polymer has numerous uses due to the insolubility of the product in organic solvents and the resistance to heat and mechanical strain. Thus, the applications of photopolymerization are wide-ranging, and encompass the automotive, electronic, medical, optical, and coating industries.

Currently, issues affecting the cure speed and overall quality of the final product (shape, size, and surface finish) are limiting the use of photopolymerization in certain applications. For example, inhibition by oxygen in free-radical polymerization leads to a significant decrease in cure speed. Another disadvantage is the inability of many lasers and UV exposure tools to homogeneously cure thick or strongly absorbing samples. Finally, the problem of shrinkage during polymerization negatively impacts applications that require accurate part shape and size. Methods for modifying processes and materials to deal with these issues are traditionally derived in one of two ways: (1) through intuition and trial-and-error experiments or (2) from predictive models to optimize materials and processes for specific applications. In many cases the complexity of light propagation, photo initiation, and polymerization, in combination with the interdependence of these processes, makes intuitive analysis and design difficult. Although rigorous predictive models for process and material design could save tremendous amounts of time and expense, their use has been limited by difficulties associated with obtaining proper parameterization. As a result, simplified models are often used to describe changes in material properties during photopolymerization.

For example, stereolithography (SL) is a process that utilizes pattern-wise UV exposure to induce polymerization of liquid monomers and thus produces three-dimensional solid objects directly from computer-aided design (CAD) files. The technology heavily relies on the use of models to correctly sequence and control the SL exposure system (i.e. a laser in most systems) to build the part to correct size and shape. Modeling of the energy deposition from the exposure source is quite rigorous using classical optical models. On the other hand, the modeling of the material response to light exposure is generally empirical. The most widely used SL process models

* Corresponding author. Tel.: +1 404 894 5134; fax: +1 404 894 2866.
E-mail address: vbreedveld@chbe.gatech.edu (V. Breedveld).

0032-3861/$ - see front matter © 2006 Elsevier Ltd. All rights reserved.
doi:10.1016/j.polymer.2006.01.095

employ a simple energy threshold: monomeric liquid is converted to solid polymer instantaneously when the local exposure dose exceeds a critical threshold value. This is a gross oversimplification of the true photopolymerization process, in which the molecular weight and crosslink density change gradually, and the predictivity of these models is generally restricted to the exact experimental conditions for which it was parameterized. In the case of SL, there is significant interest in developing processes and materials that result in higher throughput, better spatial resolution, and improved surface finishes. Making such improvements would be greatly aided by quantitatively accurate models that can capture the behavior of photopolymer resins during polymerization, and during the last decade several research groups have made significant strides forward [1–8]. One of the main problems with model development is the need for experimental validation and refinement, which is still problematic with existing techniques.

To improve existing theoretical models, experimental methods are needed that are capable of testing the model predictions with high spatial and temporal resolution. In particular, techniques capable of measuring chemical and mechanical changes during the photopolymerization process have recently attracted attention. The first time-resolved techniques for monitoring photopolymerization were molecular spectroscopy (IR [9] and Raman [10]) and calorimetry (photo-DSC [11]). Both approaches detect chemical changes within the resin on the molecular level and do not provide specific information about the evolution of mechanical properties. Calorimetry also has the drawback of long response times due to the relatively low thermal conductivity of the sample, which limits the temporal resolution of the instrument. Real-time FTIR spectroscopy has been combined with a rheometer to simultaneously monitor chemical conversion and changes in sample rheology [12–15]; however, this method does not account for spatial variations across the sample, since rheometers measure average mechanical properties over the entire sample volume. The objective of this study was to develop a set-up in which particle tracking microrheology could be employed to quantitatively monitor the changes in mechanical properties during photopolymerization. The principal advantage that microrheology has over the methods listed above is the ability to achieve excellent spatial and temporal resolution.

2. Background

In traditional rheology, bulk mechanical properties are measured by subjecting samples to an externally imposed shear stress or strain. Microrheology, on the other hand, relies on the Brownian motion of micron-sized particles embedded in the sample to assess the viscoelastic properties of the surrounding medium [16]. A typical experimental setup employs video-microscopy to track the Brownian motion of micron-sized, inert, fluorescent particles [17]. Information about the local mechanical properties of the sample is then obtained by performing statistical analysis of the tracer particle motion. For a Newtonian liquid, the motion of tracer particles is diffusive and their mean-squared displacement (MSD) is related to the sample viscosity by the Stokes–Einstein relation [18]:

$$\langle \Delta r^2(\tau)\rangle \equiv \langle |r(t+\tau)-r(t)|^2\rangle = 2dD\tau = \frac{dk_{\mathrm{B}}T}{3\pi\eta a}\tau \tag{1}$$

where the left-hand term is the MSD, k_{B} is Boltzmann's constant, T is the absolute temperature, d is the dimensionality of the particle trajectories (usually 2 for microscopy), a is the particle radius, τ is the lag time, and the brackets designate averaging over all starting times t. If the particle size is known, Eq. (1) enables viscosity measurements by monitoring the time-dependent MSD [19]. Particles in a fully elastic environment will not be able to move over long distances; instead, a maximum displacement occurs when the thermal energy is equal to the elastic energy of the deformed cross-linked network. As a result, the MSD approaches a plateau for long lag times [19]:

$$\langle \Delta r^2\rangle_{\tau\to\infty} = \frac{dk_{\mathrm{B}}T}{3\pi Ga} \tag{2}$$

where G is the elastic modulus of the elastic medium.

Complex fluids that are neither Newtonian liquids nor completely elastic, exhibit much more complex behavior including a frequency dependent complex viscoelastic modulus with both viscous and elastic components [18,19]: $G^*(\omega)=G'(\omega)+iG''(\omega)$. The fundamental basis of particle tracking microrheology in such materials is the application of the generalized Stokes–Einstein relation (GSER) for the motion of a sphere in a homogeneous, incompressible viscoelastic fluid; in the Laplace domain the GSER takes the following form [18]:

$$\langle \Delta\tilde{r}^2(s)\rangle = \frac{dk_{\mathrm{B}}T}{3\pi as\tilde{G}(s)} \tag{3}$$

where s is the Laplace frequency and $\tilde{G}(s)$ is the frequency-dependent modulus. The GSER is essential to particle tracking microrheology because it translates the measured MSD into macroscopic viscoelastic material properties. Both the viscous and elastic component can be determined from $\tilde{G}(s)$, since the real and imaginary part of $G^*(\omega)$ are related to each other through the Kramers–Kronig relations [18]. The mathematical transformation from the MSD to viscoelasticity tends to amplify experimental noise and does not add fundamental insight. For this study, we have, therefore, chosen to report transient MSD data rather than viscoelastic moduli in order to emphasize the principles of microrheology when applied to photopolymerization.

3. Experimental

The samples in this study consisted of three main components: acrylic monomer, photoinitiator, and fluorescent tracer particles for microrheology. Three commercial acrylate monomers with different functionality were used as obtained from Sartomer: ethoxylated pentaerythritol tetraacrylate (E4PETeA, SR®494), trimethylolpropane triacrylate

(TMPTA, SR®351), and triethylene glycol diacrylate (TEGDA, SR®272). A general-purpose photoinitiator, 2,2-dimethoxy-1,2-diphenylethan-1-one (DMPA, Irgacure®651, Ciba), was used as received. Silica particles containing red fluorescent dye (rhodamine) with a diameter of 0.5 μm were used as tracers [20].

After mixing the components and sonicating the samples briefly to break-up potential tracer particle aggregates, the samples were loaded into a 120 μm deep sample chamber created by placing Parafilm spacers between a microscope slide and cover slip. The samples were sealed with vacuum grease and placed on an inverted microscope. Using a 100× oil-immersion objective, the motion of the fluorescent tracer particles was tracked by capturing images from a CCD camera onto a PC. Statistical analysis of the recorded movies was performed with modified versions of image analysis routines originally coded by Crocker and Grier [21] for the software package IDL (Research Systems Inc.). After obtaining particle positions in subsequent images, particle trajectories were reconstructed and the MSD was calculated as a function of both time and lag time τ [22]. On average, 30 tracer particles were tracked simultaneously during the experiments to obtain statistically meaningful results on the in-plane Brownian motion. Diffusion perpendicular to the focal plane leads to particle loss and terminates trajectories. For highly viscous media like the acrylate monomers, this does not affect experiments; the inset of Fig. 1 shows that the tracer MSD is less than 0.3 μm for a lag time of 5 s for the liquid monomer.

Exposure of the sample to a 1000 W Hg(Xe) UV lamp (Spectra-Physics) was used to induce polymerization; illumination was controlled through a manually operated zero aperture iris diaphragm and optical filters were used to vary intensity and spectral characteristics of the light.

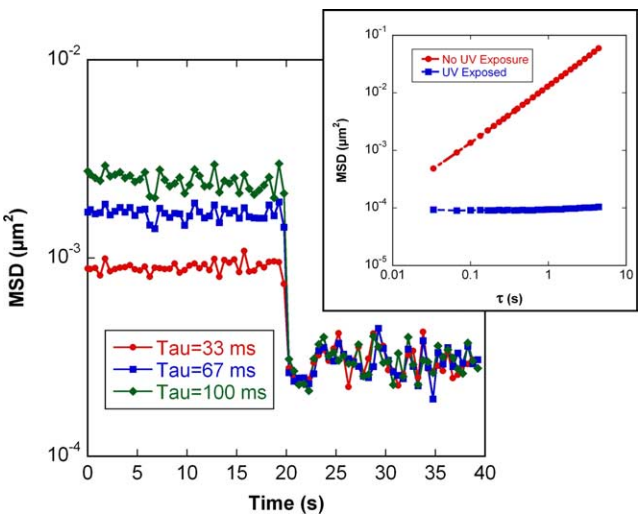

Fig. 1. Transient MSD for tracer particles in a curing sample of E4PETeA loaded with 5.0 wt% DMPA; gelation occurs at 19.8 s. The inset shows steady state results of MSD versus τ in the liquid and gel regimes.

4. Results and discussion

Initial experiments were performed on E4PETeA with 5.0 wt% DMPA to evaluate the ability of microrheology to distinguish between a liquid monomer and photopolymerized gel. The motion of tracer particles in a UV irradiated (100 s) and unexposed sample was tracked and analyzed. The inset of Fig. 1 shows that the exposed sample has a slope of zero in the double-logarithmic plot of MSD versus lag time, while the unexposed sample has a slope of one. These slopes are characteristic of an elastic gel (Eq. (2)) and a viscous Newtonian liquid (Eq. (1)), respectively. Next, a sample of the same composition was exposed to UV illumination after 6.6 s using a manually controlled shutter. A mask was used to restrict the area of illumination and minimize sample shrinkage, and a 365 nm band-pass filter (center wavelength 356 nm, half-width 15 nm) was inserted in the light path to enhance control of polymerization kinetics for modeling purposes. The transient MSD curves in Fig. 1 prove that microrheology can accurately monitor changes in sample rheology of UV irradiated photoresins. The point at which the MSD first becomes independent of τ was used to define the gelation point. Before the liquid-to-solid transition, the MSD increases with increasing lag times, characteristic of a viscous liquid. After the transition the MSD is independent of lag time, which is the signature of an elastic gel (see inset). Other definitions of gel point based upon the classic Winter–Chambon gelation theory [23] were examined and yielded comparable gelation point data. Fig. 1 also shows that exposure to UV light initially causes no significant changes in MSD; the sample viscosity apparently does not change significantly during the initial stages of photopolymerization. After 19.8 s (13.2 s of UV exposure), a sudden liquid-to-gel transition occurs, which could easily be captured with particle tracking microrheology.

The small depth of focus of the microscope, in combination with accurate manipulation of its location via the fine focus, enabled measurements of polymerization with high spatial resolution. In particular, the gelation transition could be studied as a function of UV penetration depth into the sample (the distance from the illuminated resin surface to the focal plane). For these experiments, samples of E4PETeA were loaded with different concentrations of DMPA initiator and the microscope was focused at the illuminated top surface of the sample chamber (zero penetration depth), before moving the focal plane to the desired location. Fig. 2 shows that gelation time increases by an approximate factor of two across a sample depth of 120 μm, independent of initiator concentration. To investigate if this depth-dependent gelation was due to oxygen inhibition reactions, E4PETeA with 0.25 wt% DMPA was degassed under vacuum. Comparison of the deoxygenated and oxygenated samples with 0.25 wt% in Fig. 2 shows that oxygen slows down the photopolymerization process significantly, but that it is not the cause of inhomogeneous cure across 100 μm samples. The error bars in Fig. 2 are mainly the result of using a manual shutter to control the UV illumination.

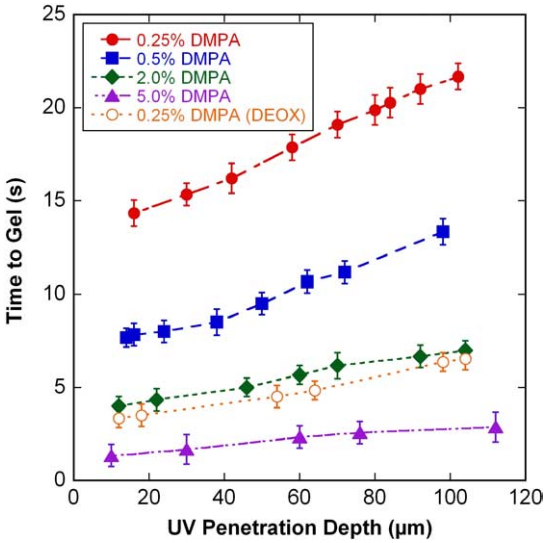

Fig. 2. Plot of gelation time as a function of UV penetration depth for E4PETeA with 5.0, 2.0, 0.5, and 0.25 wt% (both oxygenated (●) and degassed (○)) DMPA cured using 365 nm UV irradiation. Lines are to guide the eye.

The variations in gel time across the sample cannot be fully explained by absorption either. Beer's law predicts the exponential decay of the amount of photons delivered to the sample with increasing thickness of the absorbing medium, thus limiting the initiation reactions of free-radical photopolymerization at greater penetration depth. For E4PETeA, at 5.0 wt% DMPA 63% of the light penetrates to the bottom of a 100 μm thick sample [4], while at 0.25 wt% almost 100% of the incident light reaches the bottom; nevertheless, the gelation variations for the 0.25 wt% samples are significant.

The measurements were repeated with monomers of different functionality. TEGDA (bifunctional) and TMPTA (trifunctional) with 5.0 wt% DMPA were cured using 365 nm UV irradiance and the results are compared to the data for E4PETeA (tetrafunctional) in Fig. 3, which confirms that the

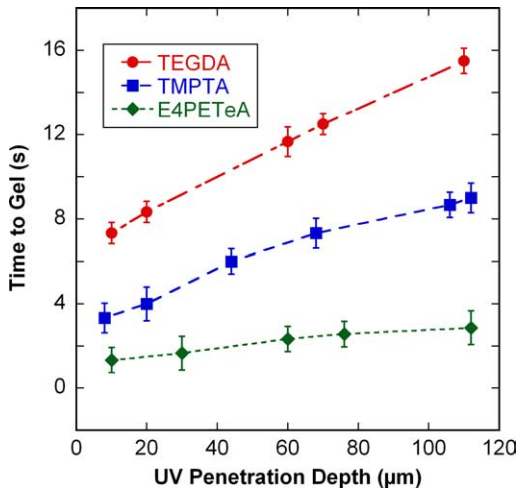

Fig. 3. Plot of gelation time as a function of UV penetration depth for three different acrylate monomers: TEGDA, TMPTA, and E4PETeA with 5.0 wt% DMPA and cured using 365 nm UV irradiation. Lines are to guide the eye.

trend observed for E4PETeA in Fig. 2 is independent of functionality. As expected, monomers with higher functionality form cross-linked networks at lower conversions of the polymerizable functional groups; therefore, highly functional monomers require shorter times to reach the point of gelation.

As mentioned previously, the energy threshold model, which assumes that gelation occurs once a critical energy dose threshold is reached, is often the starting point for photopolymerization models discussed in the literature [1–3]. For continuous irradiation (i.e. continuous initiation of polymerization) of a sample in which the polymerization reaction time scale for each initiation event is fast compared to the gelation time scale, the critical energy threshold should be the product of gelation time and UV intensity:

$$E_{cr} = I_a t_{gel} \tag{4}$$

where the UV intensity at a given depth, I_a, is defined by Beer's law as:

$$I_a = I_0\, e^{(-kx)} \tag{5}$$

k being the absorption coefficient, and x the distance below the surface illuminated with intensity I_0. These conditions should be met in the case of the free radical polymerization experiments reported here since at conversions below the gel point the lifetime of active radicals should be much less than 1 s while the gelation time scales are on the order of seconds at the reported light intensities. According to Eqs. (4) and (5), the gelation time should scale as $t_{gel} \sim e^{(kx)}$. The profiles in Figs. 2 and 3 appear to deviate from this exponential prediction. Over the available depth range (working distance of 100× objective), however, it is difficult to differentiate between linear and exponential scaling. To evaluate the accuracy of the threshold model in more detail, the illumination intensity I_0 was varied by inserting various neutral density filters in the light path: ND10 (10% transmission), ND03 (50% transmission), and ND01 (78% transmission). Samples of E4PETeA loaded with 5.0 wt% DMPA were exposed to UV light at 365 nm and, as expected, Fig. 4(A) shows that decreasing the UV intensity increases the required gelation time considerably. Given that both the material constant k and location x are controlled between experiments, the gelation time should scale with the inverse of the incident intensity, $t_{gel} \sim 1/I_0$. Therefore, it should be possible to collapse the data in Fig. 4(A) onto a single master curve by normalizing gelation times by the filter transmittance. Deviations between the normalized and unfiltered data in Fig. 4(B) show that the critical energy threshold model becomes progressively more inaccurate at low incident light intensity and for thick samples, which was also visible in Figs. 2 and 3. The main reason for failure of the simple threshold model under these conditions is that the model completely neglects reaction kinetics; for slow reactions, the balance between initiation, propagation and termination reactions becomes increasingly important. These experimental results show that microrheology is capable of capturing previously inaccessible details on photopolymerization and support the need for inclusion of reaction kinetics in

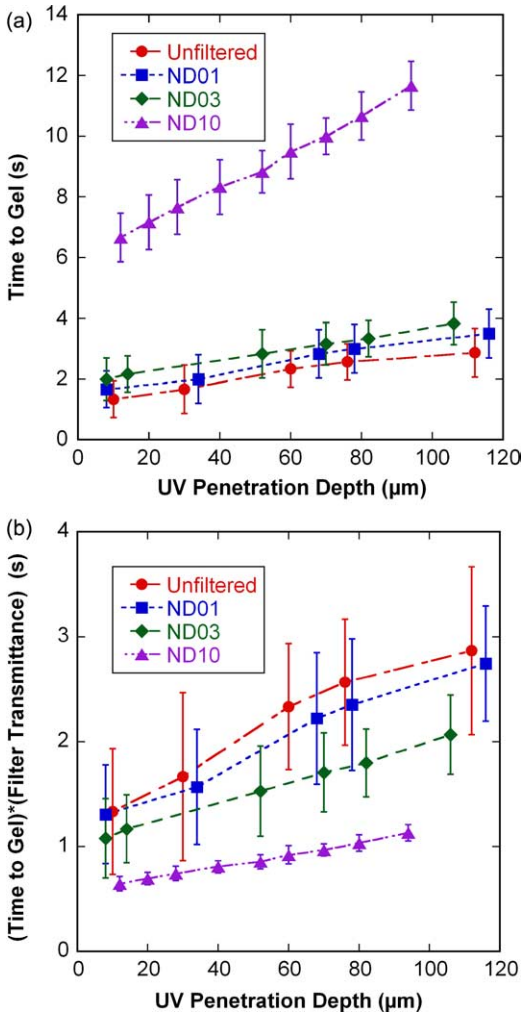

Fig. 4. (A) Plot of gelation time as a function of UV penetration depth and incident intensity for E4PETeA with 5.0 wt% DMPA, using 365 nm UV irradiance. (B) Plot of same data after normalization with filter transmittance.

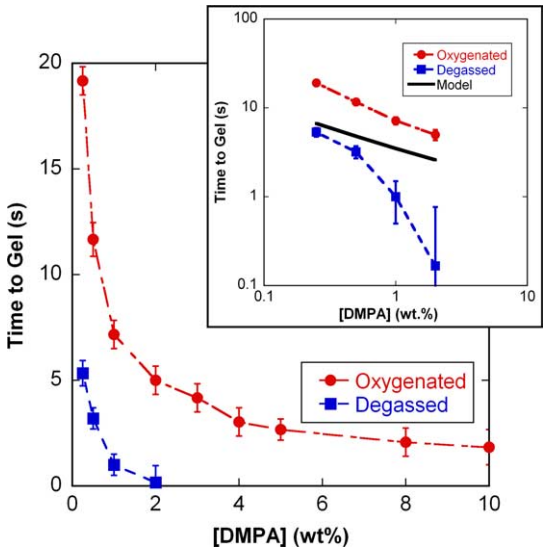

Fig. 5. Plot of gelation time as a function of DMPA loading concentration for both oxygenated and degassed samples of E4PETEA cured using 365 nm UV irradiance. Lines are to guide the eye, except for the model in the inset.

photopolymerization models. However, a detailed evaluation of various models is beyond the scope of this communication.

To further elucidate the role of reaction kinetics, the effects of initiator concentration and oxygen inhibition were studied. A fraction of the samples was degassed under vacuum and loaded into sample chambers in an oxygen-free environment. All of these samples were cured using 365 nm UV illumination and gelation was determined at a standard depth of 60 μm from the illuminated surface. Fig. 5 shows how the gelation time of E4PETeA depends on the initiator concentration: after a strong decay at low initiator concentrations, the gelation time levels off around 4.0 wt% for the samples with oxygen. Significant impact of oxygen inhibition is also evident, supporting the results in Fig. 1: the deoxygenated samples undergo gelation much more rapidly than their counterparts with oxygen. For example, at 2.0 wt% DMPA gelation occurs nearly instantaneously. In the inset, the data are replotted on a double logarithmic scale to highlight the fact that oxygenated samples follow power-law scaling of gelation time with initiator concentration; the degassed samples show a much stronger decay, which can best be described as exponential. In addition, the inset shows a direct comparison of experimental data to model predictions made using a model developed by Tang and coworkers. [4] This model is a comprehensive photopolymerization model that incorporates both heat and mass transfer and free radical polymerization reactions including initiation, propagation, and termination. This model was carefully parameterized experimentally for a series of different photopolymer resins including the resin used in this paper. The model was parameterized using experiments conducted in a nitrogen purged environment, and thus an oxygen inhibition model was not directly parameterized for this model. The accuracy of the model was validated by utilizing it to quantitatively predict the results of stereolithography photopolymerization experiments. Utilizing stereolithography experiments, the critical degree of polymerization that results in gelation was determined. Calculations were also performed using the photopolymerization model including oxygen inhibition, employing rate constants for similar resins from the literature. However, these oxygen inhibited model predictions did not deviate significantly from the predictions without oxygen inhibition and thus are not shown in the graphs. It is obvious that the microrheology experiment is quite sensitive to the presence of oxygen, and thus work is in progress to utilize this data in conjunction with a comprehensive photopolymerization model to extract parameters for oxygen inhibition that can properly capture this behavior. These oxygen inhibition model results will be compared to differential photocalorimetry experiments conducted in controlled environments containing known concentrations of oxygen.

The experimental results from the microrheological study provide excellent data with high spatial resolution. Such detailed results can be used to optimize and refine

photopolymerization models, because of the ability to make detailed comparisons with model predictions. Combining depth profiling experiments with variations of initiator and inhibitor concentrations in the samples will facilitate the determination of model parameters, such as kinetic rate constants for propagation, termination and inhibition. Current techniques are apparently not sensitive enough to accurately determine all rate constants in the reaction pathway, as is shown by the discrepancies between experimental results and model predictions. Although the parameters used in the acrylate photopolymerization model have previously been shown to provide reasonable agreement with the differential photocalorimetry (DPC) and stereolithography part shape measurements [4], the more stringent comparison with microrheology data over a wide range of initiator concentrations reveals the limitations of this model. Studies are currently underway to understand which model parameters may be relatively insensitive to the methods currently used to parameterize the photopolymerization model and which can be better estimated by additional fitting of the model to the microrheology data. Work is also in progress as mentioned previously to model the effect of oxygen quenching observed experimentally in the microrheology experiments by parameterizing the quenching mechanisms in the existing radical photopolymerization model [4].

5. Conclusions

The results presented prove that microrheology is an effective tool for monitoring photopolymerization. The important liquid-to-gel transition can be determined with high spatial and temporal accuracy and thus provides unprecedented experimental insight. The results can be used to directly test photopolymerization models and enhance the understanding of photo-induced free-radical polymerization. The role of oxygen inhibition, initiator concentration and UV illumination were investigated for acrylate resins. It was shown that the popular energy threshold model is not sufficient to explain our experimental results. Future optimization of the experimental method will include the use of electronic shutters to minimize experimental errors.

Acknowledgements

We are grateful to the GAANN Program in Polymer Science and Engineering at Georgia Tech for financial support and to Yanyan Tang and Gökcen Altun for the model discussions.

References

[1] Brunner TA, Ferguson RA. Solid State Technol 1996;39:95.
[2] Ahn N, Kim B, Baik H. Optical microlithography XI. Proc SPIE 1998; 3334:752.
[3] Cobb N, Zakhor A. Optical microlithography X. Proc SPIE 1997;3051: 458.
[4] Tang Y, Rosen DW, Muzzy JD, Henderson CL. Submitted for publication.
[5] Goodner MD, Bowman CN. Chem Eng Sci 2002;57:887.
[6] Dickey MD, Burns RL, Kim EK, Johnson SC, Stacey NA, Willson CG. AIChE J 2005;51(9):2547–55.
[7] Lovestead TM, O'Brien AK, Bowman CN. J Photochem Photobiol A 2003;159(2):135.
[8] O'Brien AK, Bowman CN. Macromolecules 2003;36(20):7777.
[9] Lin Y, Stansbury J. J Am Chem Soc 2001;42:809.
[10] Nelson E, Scranton A. J Raman Spectrosc 1996;413.
[11] Clark S, Hoyle C, Jonsson S, Morel F, Decker C. Polymer 1999;40:5063.
[12] Chiou B, English R, Khan S. Macromolecules 1996;29:5368.
[13] Chiou B, English R, Khan S. Macromolecules 1997;30:7322.
[14] Lange J. Polym Eng Sci 1999;39:1651.
[15] Botella A, Dupuy J, Roche A. Macromol Rapid Commun 2004;25:1155.
[16] Gardel ML, Valentine MT, Weitz DA. In: Brues KS (ed.), Microscale diagnostic techniques 2005 Springer New York
[17] Mukhopadhyay A, Granick S. Curr Opin Colloid Interface Sci 2001;6: 423.
[18] Breedveld V, Pine D. J Mater Sci 2003;38:4461.
[19] Waigh TA. Rep Prog Phys 2005;68:685.
[20] Tolpekin VA, Duits MHG, van den Ende D, Mellema J. Langmuir 2003; 19:4127.
[21] Crocker J, Grier D. J Colloid Interface Sci 1996;179:298.
[22] Sato J, Breedveld V. J Rheol 2006;50(1):1.
[23] Winter HH, Chambon F. J Rheol 1986;30:367.